First Annual Report Grant NGR06-002-102

by

Thomas H. Vonder Haar
Colorado State University

December 1971

FIRST ANNUAL REPORT

for

Grant NGR 06-002-102

Radiation Measurements from Polar and Geosynchronous Satellites

Period: 1 October 1970 - 30 September 1971

Prepared by

Thomas H. Vonder Haar, Principal Investigator

Department of Atmospheric Science

Colorado State University

for

NATIONAL AERONAUTICS AND SPACE ADMINISTRATION

Contracting Officer: J. R. Jishow

Technical Monitor: W. R. Bandeen

December 1971

TABLE OF CONTENTS

SUMMARY

During the first year of research under Grant NGR 06-002-102, we have eight final papers and publications to report. They refer to new measurements of the earth's radiation budget; its climatology and its interannual variation. In addition, preliminary results deal with ocean energy transports, specific large scale and local radiation budget anamolies, and studies of the separate radiation budgets of the atmosphere and ocean. Initial work in preparation for additional radiation budget measurements from EOS and ATS satellites is described. A radiation budget system simulation program and several smaller projects (including a radiance normalization technique) complete the report. First "annual" global maps of the earth's radiation budget as measured from NIMBUS-III are included among 17 figures.

I. INTRODUCTION TO GRANT OBJECTIVES

The purpose of this research grant is to study the earth's radiation budget using measurements from meteorological and earth survey satellites. Time and space scales covered depend on the specific atmospheric problem under study. At largest and longest scales the measurements from satellites allow study of climate of the globe and its distinct hemispheres; for latitude zones during specific seasons the data specify the fundamental forcing that drives our ocean and atmosphere; over local regions, the energy exchange between earth and space affects local physical energetics as well as biological processes.

Using the data from our first generation satellites, as well as new data currently being gathered from the NIMBUS series, we can do much more than acquire a radiation climatology; we can study the feedback and interactions between the radiation patterns of our earth-atmosphere system and the activity of our fluid circulations that modulate, and sometimes amplify, the energy exchange.

In addition, grant objectives include study of the potential of new satellite data for improving our information base regarding the earth's radiation budget, and for allowing scientific studies not previously possible. Data sampling and engineering factors related to future satellite systems are given preliminary conceptual study. Some satellite platforms, especially geosynchronous, can serve both to measure the radiation budget and to acquire basic information about the concurrent and subsequent mass and wind structure of the atmosphere.

II. SCIENTIFIC RESULTS

1. Final Results Included in Publications and Papers

One means of evaluating Grant progress during the first year is a survey of the research work that has traveled full circle from raw satellite data to refereed scientific publication. Appendix A lists the eight (8) papers and publications sponsered by the Grant this year. It also includes remards to place each entry in perspective.

We have, no less, obtained the first moderately high resolution measurements of the earth's radiation budget and its components during four consecutive seasons and for the "annual" case derived from them. (See the three large Fig., 1, 2, and 3 attached). This has been done in collaboration with several members of the Laboratory for Meteorology and Earth Science, especially Mrs. Musa Pasternak.

In addition, the grant allowed partial support of a lengthy visit by a scientific colleague and consultant, Dr. Ehrhard Raschke, whose work with the NIMBUS-II satellite data provided the basic data reduction plan for NIMBUS-III. Besides successful data processing, it is important to note that complete documentation and discussion of the data reduction techniques and assumptions is included in the reporting documents. Thus, if future information allows refinement of the processing, this can be done.

On the global, hemispheric and zonal scales, the NIMBUS-III results (for both seasonal and annual samples) confirm results from earlier satellite experiments (Vonder Haar and Suomi 1969, 1971). They too show a warmer and darker planet than had been estimated by computations using climatological data (Fig. 4).

Geographical distributions of the radiation budget also show relative minima in the energy gain over land and oceanic deserts of the tropics (Fig. 3).

Zonal averages from all satellites available thus far show that most of the extra energy entering our system is arriving in the tropics 0-20^{o}. (Fig. 5, note the albedo, lower curve; open circles are London (1957), solid line (Vonder Haar and Suomi, 1971), dashed line, NIMBUS-III "annual").

Even before the confirming NIMBUS-III results were ready, estimates based on calculations (e.g., London and Sasamori (1971)) had already been revised to agree with the earlier satellite measurements (Fig. 6). Now they have even more reason to do so, and by fixing their upper boundary to the measurements, the calculations within the atmosphere should be more accurate. It is now apparent that we have measured the radiation budget of the earth atmosphere system with more absolute and relative accuracy than it can be calculated or parameterized.

SEASON	NIMBUS-III 1969-1970	SATELLITES 1962-1966	NIMBUS-II 1966
MAM	.35, 29%, −.01	.33, 30%, 0.00	
JJA	.35, 28%, −.01	.34, 26%, 0.00	.34, 31%, −.02
SON	.35, 28%, 0.00	.34, 28%, +.01	
DJF	.34, 29%, +.02	.33, 31%, +.01	
ANNUAL	.34, 29%, 0.00	.34, 30%, 0.00	——

FIRST VALUE: OUTGOING LONGWAVE RADIATION (cal cm^{-2} min^{-1})

SECOND VALUE: PLANETARY ALBEDO (percent)

FIGURE 4

THIRD VALUE: NET RADIATION (cal cm^{-2} min^{-1})

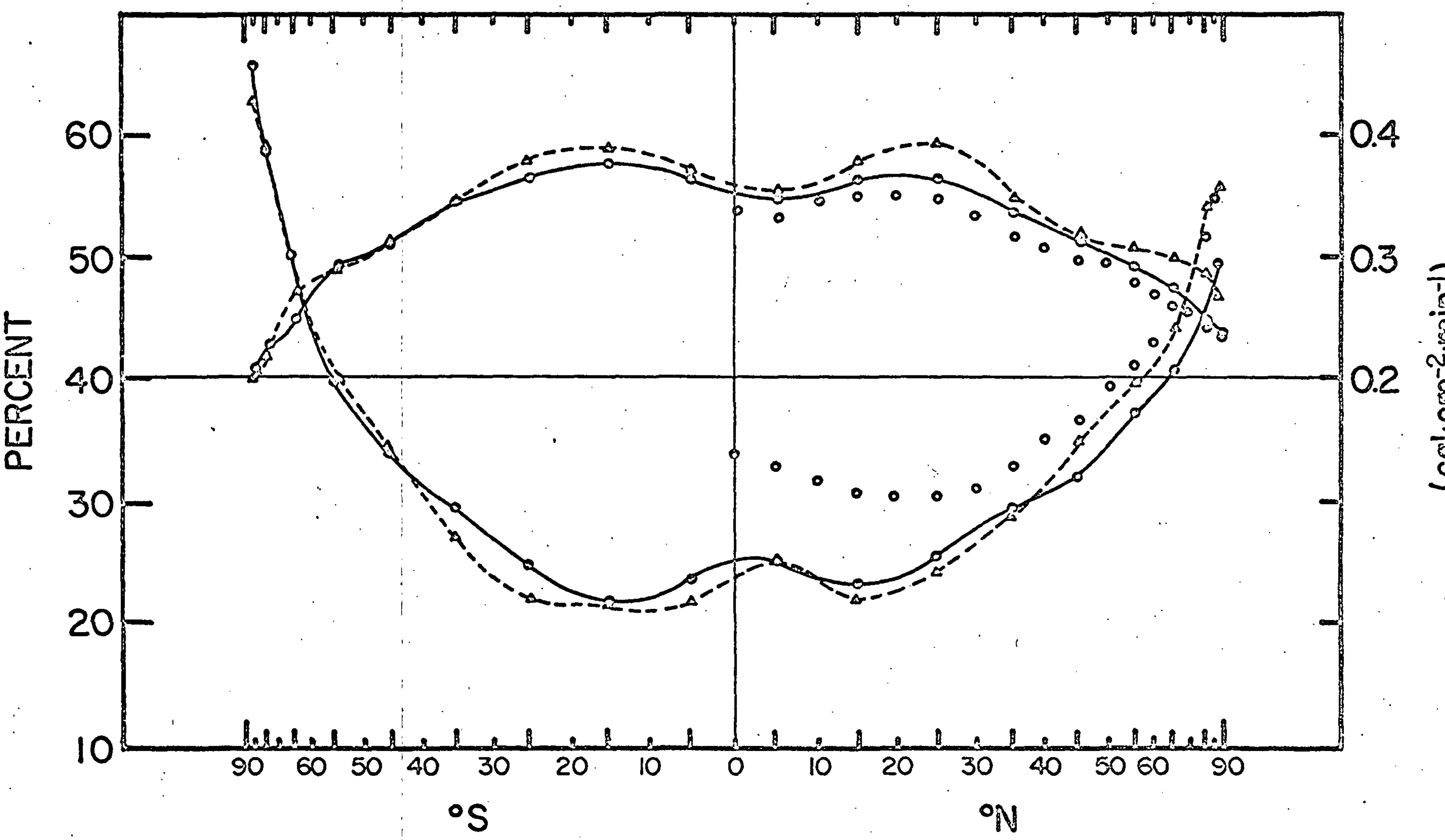

PERCENT
60
50
40
30
20
10
0.4
0.3
0.2
(cal·cm^{-2}·min^{-1})
90 60 50 40 30 20 10 0 10 20 30 40 50 60 90
°S
°N

FIGURE 5

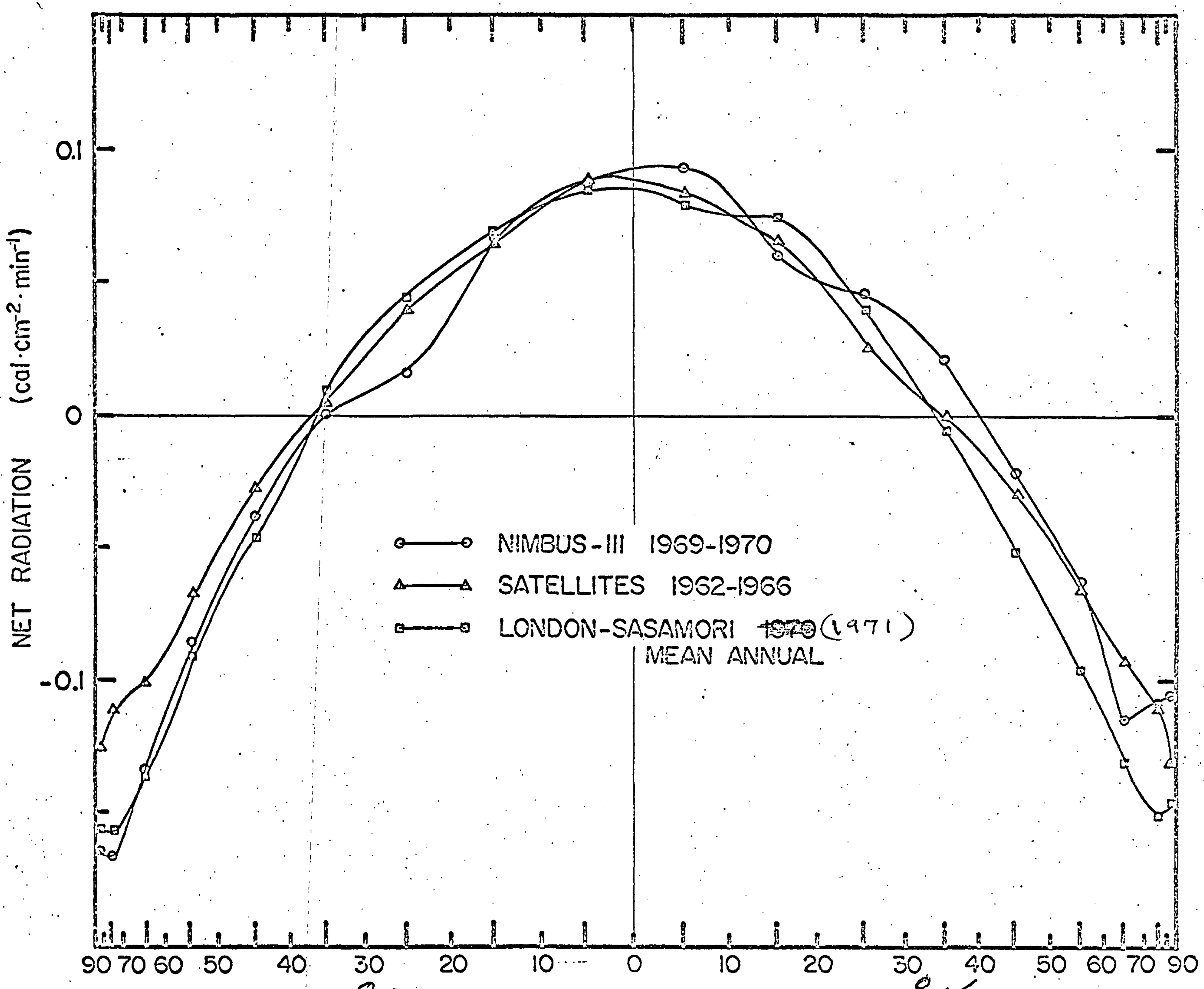

NET RADIATION (cal·cm⁻²·min⁻¹)
0.1
0
-0.1
NIMBUS-III 1969-1970
SATELLITES 1962-1966
LONDON-SASAMORI ~~1970~~ (1971)
MEAN ANNUAL
90 70 60 50 40 30 20 10 0 10 20 30 40 50 60 70 90

2. Preliminary Results of Additional Grant Research

In addition to the basic NIMBUS-III work noted above and in Appendix A, detailed study of the new (and older) radiation budget data, as well as consideration of improved sensing systems, has lead to some results not yet published, but included in the following sections.

A. Regarding the Mean Annual Radiation and Energy Budgets of the Atmosphere and Ocean

The total energy transport (in all forms) by all mechanisms (atmosphere and ocean) can be obtained from satellite radiation measurements. From Fig. 8 of Vonder Haar and Suomi (1971), the RT curve shows a transport over the northern hemisphere for the "mean annual" case shows a transport requirement for 2 x 10^{23} cal per year. In the same issue of JAS, Oort (1971) presented calculations of total atmospheric energy transport (all forms; latent heat, sensible heat, potential energy and kinetic energy) for the mean annual case. Integration of his curve (analogous to the ΔC curve of Fig. 8 in V-S) gives 1.2 x 10^{23} cal/yr. Thus, the remaining northward transport - by the ocean - must be 0.8 x 10^{23} cal/yr.

We have derived required ocean transport with the aid of satellite data and it is 40% of the total in the Northern Hemisphere. Historical estimates were as low as 10%; recent climatologies (e.g., Sellers (1965)) say 25%; we obtain 40%. Indeed, since we have already shown that the total absolute energy transport of our warmer and darker planet is greater than believed in pre-satellite days, we are finding the need for oceans in the Northern Hemisphere to transport a greater percentage of a larger absolute value - much more energy than was previously believed.

Moving primarily at the same potential level and having no latent energy, the oceans must move almost all of their energy in the form of sensible heat transport:

$$SHF = \rho c_p \int_{z_o}^{z} \overline{V} \cdot \nabla T \, dz$$

Why were the earlier estimates too low? Was z, the depth of the mixed layer, too small?; perhaps the currents, $\overline{V}$, are stronger; are the temperature gradients actually greater than assumed?

We now measure the global, integral radiation budget with a relative accuracy of 2-3%; absolute accuracy of, at best, $\pm 0.01 \text{ cal}\cdot\text{cm}^{-2}\cdot\text{min}^{-1}$. How well must we measure in order to detect climate change?

- Assume 1000 mb atmosphere plus 100 m of ocean (covering 70% of earth area) are thermally coupled.

- Assume a natural global temperature variation of $1^{o}C$/100 yr; allow sudden (short-term) climate change to have a rate of $1^{o}C$/10 years.

The energy equivalent of the latter rate is 3% of one-fourth the solar constant/10 years. The available solar energy is 70% of one-fourth the solar constant; thus, we must be able to measure with a precision of at least 4% of the available solar energy per 10 years. This is ±100 microwatts per cm^2 per year; we can do it.

B. Interannual Variations of the Energy Exchange with Space

Radiation budget measurements over a five-year period were studied by Vonder Haar and Suomi (1971) - consider these data the "normal" standard. How do the NIMBUS-III measurements compare to this norm? On a global and hemispheric scale Figure 4 shows good overall agreement, even with respect to a weak seasonal variation of the global budget.

Figure 7 shows the zonal average profiles of net radiation measured from NIMBUS. Details of this figure offer much for study. However, the simple index of equator-to-pole gradient $RN_{E/P}$ of V-S can be used to assess the strength of the forcing function in each reason. In Figure 8, the open circles denote NIMBUS-III index values, plotted against the mean and range of "normal" data. Apparently the southern hemisphere was very normal in its energy exchange between earth and space. The northern hemisphere, especially in fall and winter of 1969-70 was anomolous. Why?; what was the feedback??

An illustration of the inferences possible from satellite measurements of the radiation gradient is seen in Figure 9. Here the values obtained from the 1st generation satellites are displayed against two ordinates: the mean thermal wind (V_T) from 20^o-70^oN, 1000-300 mb and the non-dimensional thermal Rossby Number, R_{OT} (the latter provides a link between the satellite studies and dishpan experiments). Although no direct relation should be inferred, the relation between radiative forcing and circulation response is apparent. It needs further study.

On an expanded geographical scale, Figure 10 shows interannual variations of the mean seasonal infrared radiation to space (11 seasons from 1st generation satellites). Some features are easy to explain; such as the "high" range of infrared energy to space over the monsoon region of India. Relative highs in the Southeastern Pacific and southeast of Argentina and the "low" centered over the British Isles need more thought. Perhaps the latter could be caused by persistent natural cirrus. How would SST's affect this region of relatively low natural variation?

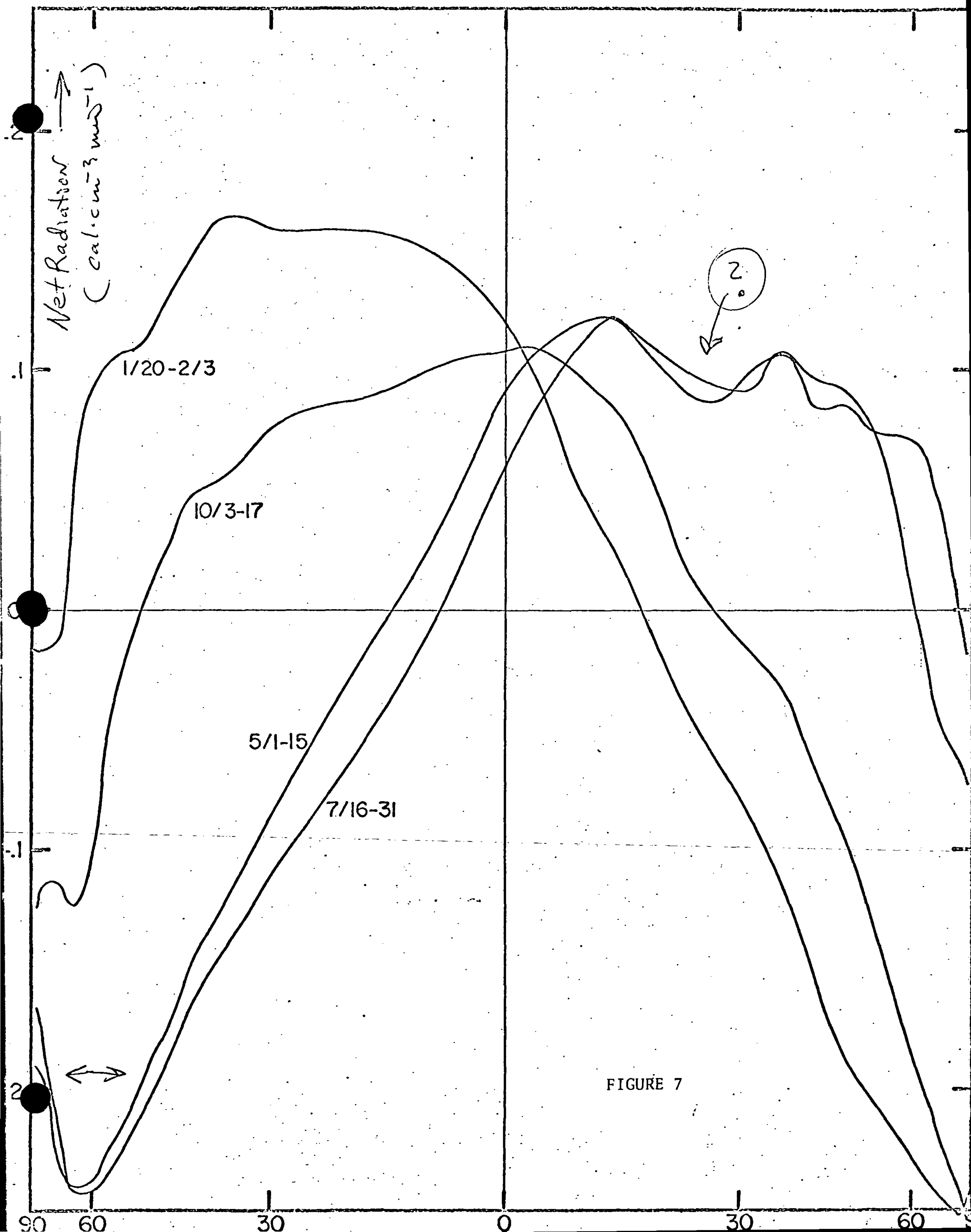

Net Radiation (cal·cm⁻² min⁻¹)
.2
.1
0
-.1
-.2
1/20-2/3
10/3-17
5/1-15
7/16-31
90
60
30
0
30
60

FIGURE 7

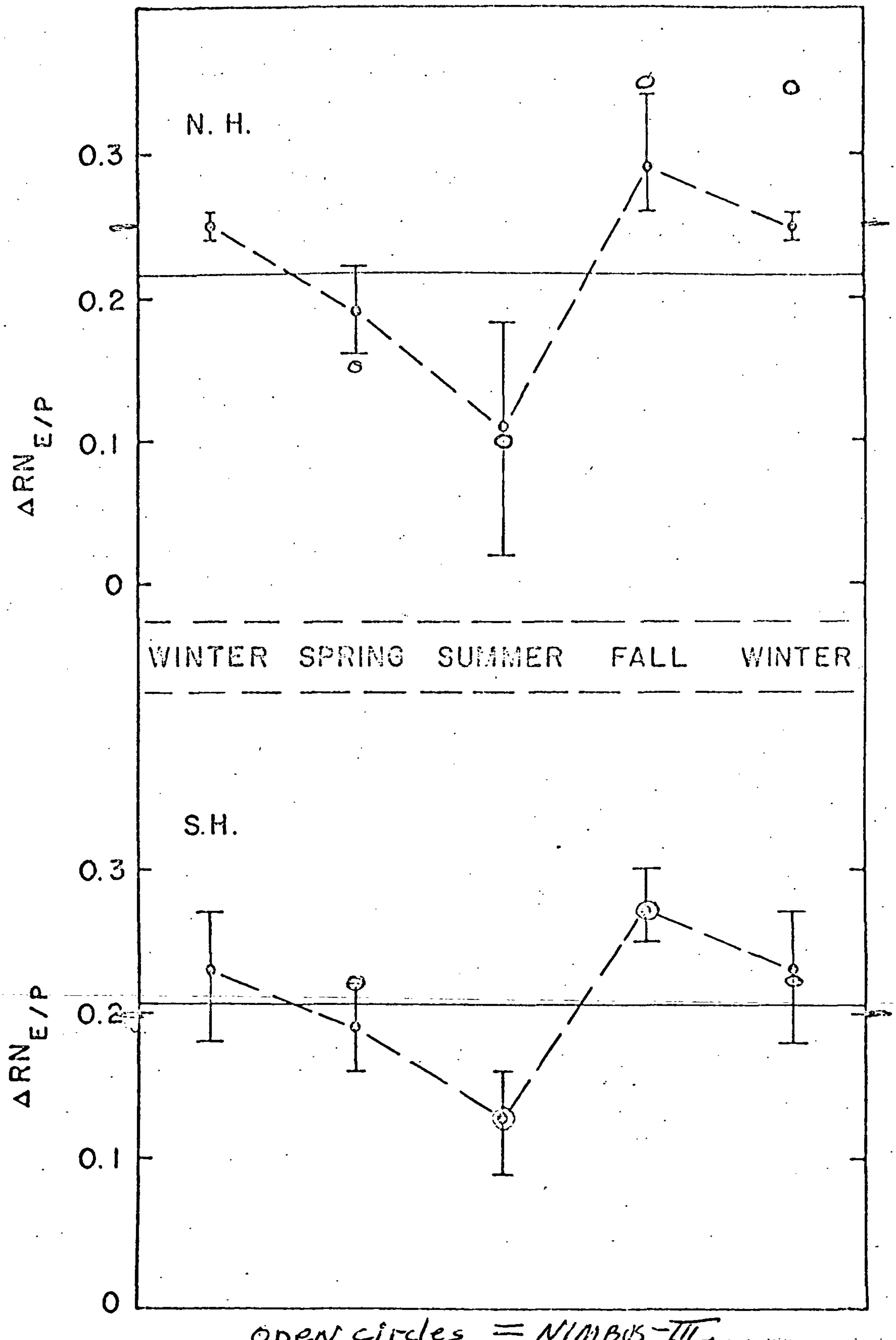
N. H.
0.3
0.2
0.1
0
ΔRN E/P
WINTER
SPRING
SUMMER
FALL
WINTER
S.H.
0.3
0.2
0.1
0
ΔRN E/P
open circles = NIMBUS-III

FIGURE 8

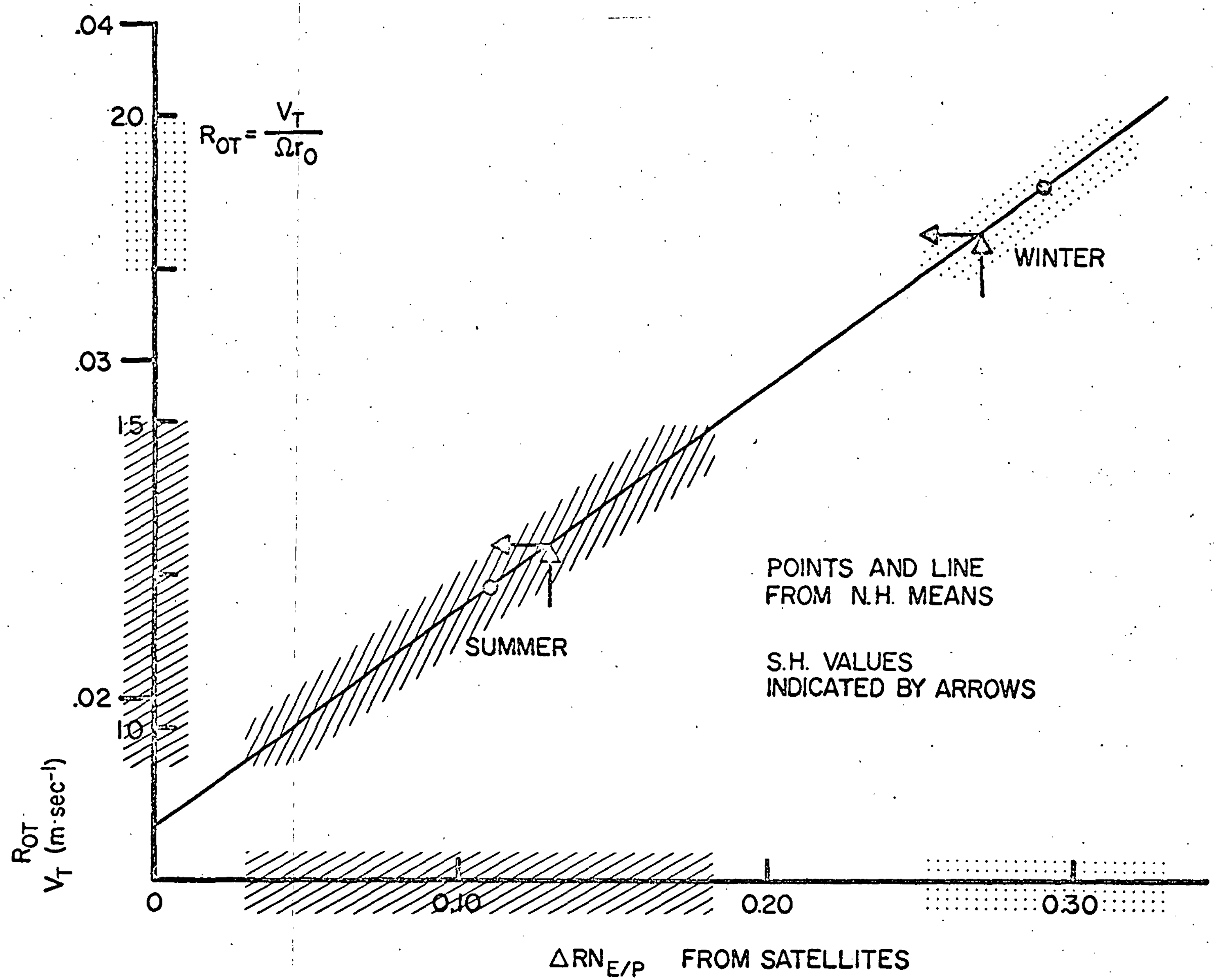

.04
20
$R_{OT} = \frac{V_T}{\Omega r_0}$
.03
1.5
.02
1.0
R_{OT}
V_T (m·sec^{-1})
WINTER
SUMMER
POINTS AND LINE
FROM N.H. MEANS
S.H. VALUES
INDICATED BY ARROWS
0
0.10
0.20
0.30
$\Delta RN_{E/P}$ FROM SATELLITES

FIGURE 9

RANGE OF TOTAL INFRARED RADIATION MEASURED FROM SATELLITES (1963-1965)

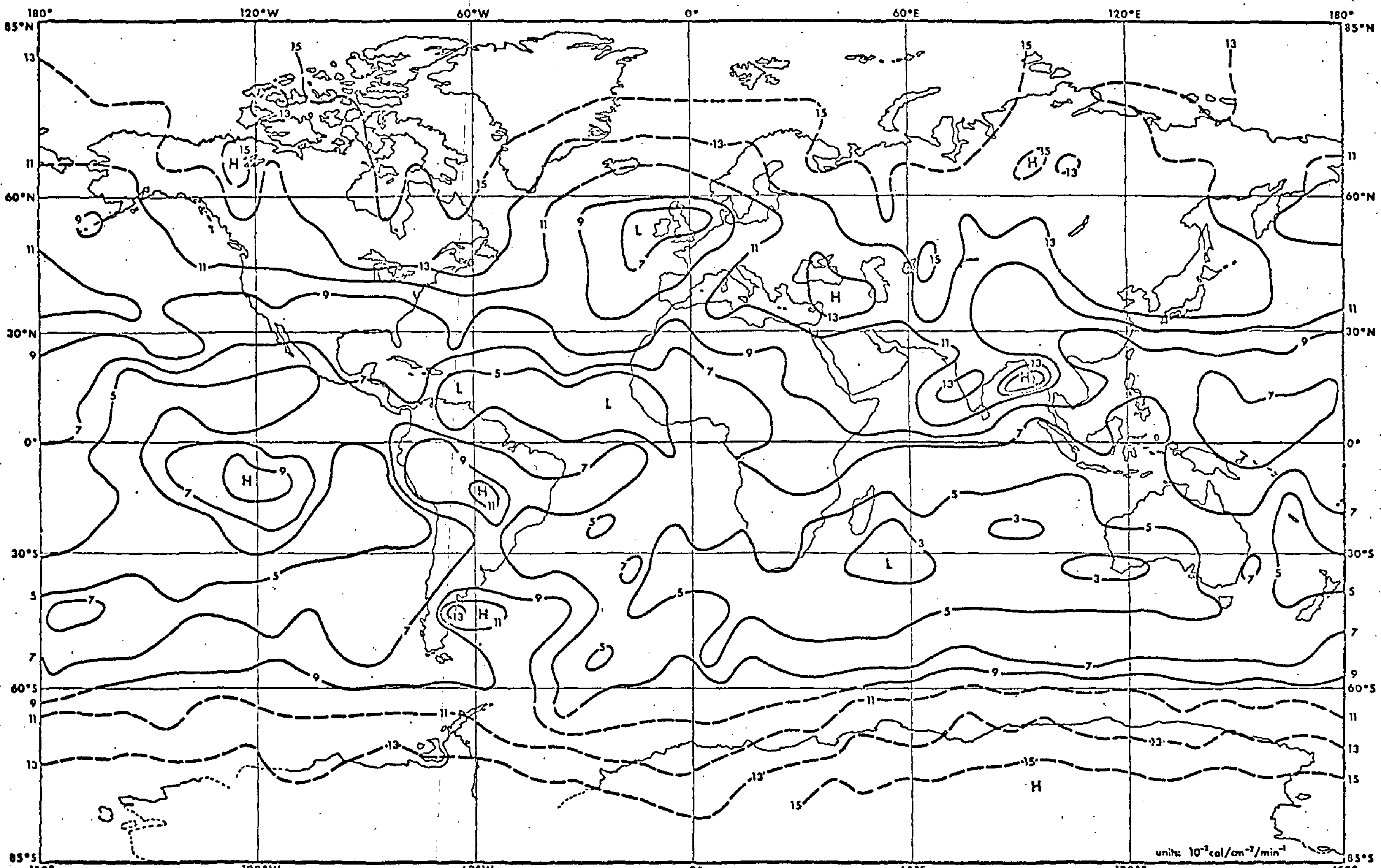

FIGURE 10

C. Separation of the Radiation Budgets of the Atmosphere and the Ocean

Attention is drawn here to polar regions where atmosphere and ocean are de-coupled during much of the year. This is under study, but the tropics, site of much current research and planning, were also considered. Satellite measurements prompted Figure 11, a reappraisal of the radiation budget of the zone 0-20°N. Here satellite, surface (solar) pyranometer, and balloon (IR) radiometersonde measurements were all used. The resulting departure from old (calculated) values is shown in both the relative and absolute sense. Such radiation considerations bound the hypothesis for organized weather systems in the tropics; they relate directly to planning for the GARP Atlantic Tropical Experiment (GATE). From satellite results already on hand it is apparent that the 1958 work of Riehl and Maldus must be revised to require more "hot towers".

As a goal for the future - determination of the true diabatic heating of the atmosphere - we show Figure 12. From it, we note that the forcing function for the developing numerical models seems to come from a random number generator! We can improve on this.

D. Application of Geosynchronous IR Imager and Temperature Sounder Data

The princiapl investigator has been a proponent of geosynchronous temperature sounder measurements for some time; once images are available in time from such a spacecraft, "snapshots" from polar orbiters suffer in comparison for many scientific studies.

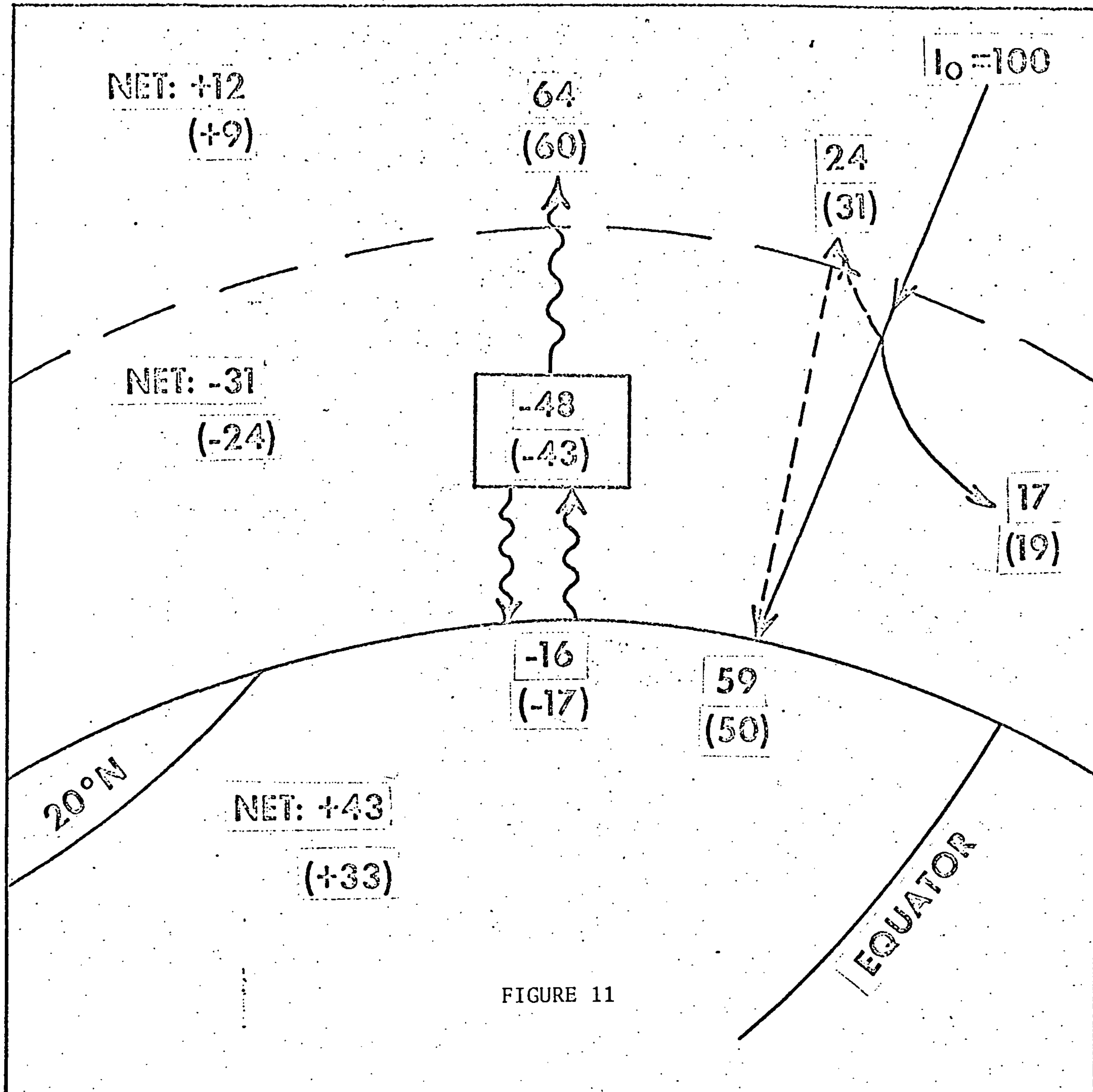

FIGURE 11

ANNUAL BUDGET 0-20°N	I_o	OCEAN+ATMOSPHERE RN_{OA}	OCEAN+ATMOSPHERE Q_r	OCEAN+ATMOSPHERE RL_{OA}	OCEAN RN_O	OCEAN Q_O	OCEAN NRL_O	ATMOSPHERE RN_A	ATMOSPHERE $Q_{\bar{A}}$	ATMOSPHERE NRL_A
'NEW'	.58	+.07	°.14	°.37	.25	°.34	-.09	-.13	.10	°-.28
(OLD)	.58	+.05	.18	.35	.19	.29	-.10	-.14	.11	-.25
RELATIVE CHANGE	0	+28%	-22%	+8%	+25%	+15%	0	+22%	0	+11

radiation units: $cal/cm^{-2}/min^{-1}$ °measured

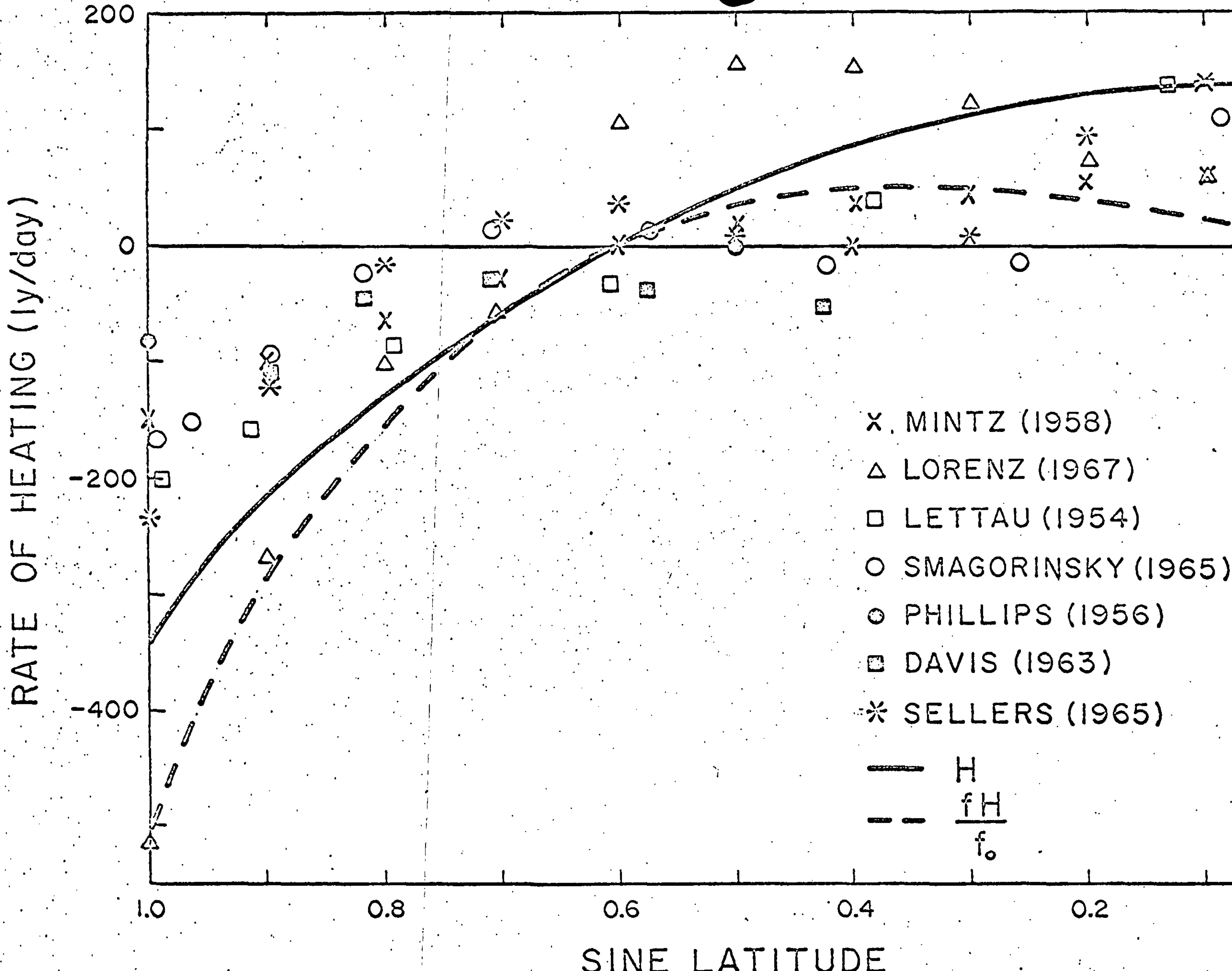

200
0
-200
-400
RATE OF HEATING (ly/day)
1.0
0.8
0.6
0.4
0.2
0.0
SINE LATITUDE
X MINTZ (1958)
△ LORENZ (1967)
□ LETTAU (1954)
○ SMAGORINSKY (1965)
○ PHILLIPS (1956)
□ DAVIS (1963)
✳ SELLERS (1965)
H
fH / f₀

FIGURE 12

Questions arise - can we detect incipient "cloud clusters" before the liquid water appears by using large scale vertical motions computed by the adiabatic technique (with a radiative adjustment) and moisture sounder? What form of the "balance" equation really applys in mid and upper levels of the tropical atmsophere. Figure 13 shows the relation between wind and mass field (via the thermal wind) as it varies with latitude.

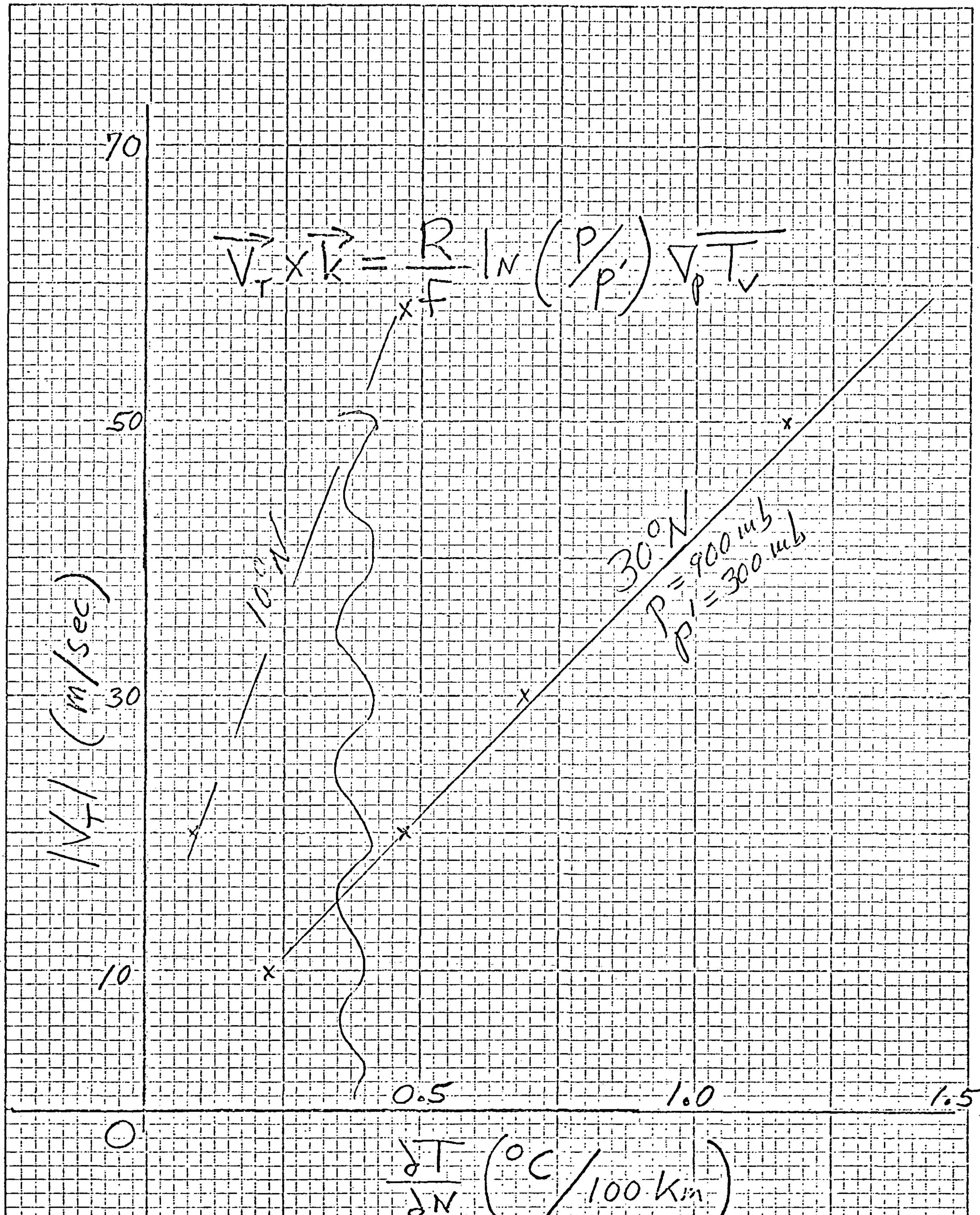

$\vec{V}_T \times \vec{k} = \frac{R}{f} \ln\left(\frac{p}{p'}\right) \nabla_p \overline{T_v}$
70
50
30
10
0
0.5
1.0
1.5
$|V_T|$ (m/sec)
$\frac{\partial T}{\partial N}$ (°C/100 Km)
10°N
30°N
p = 900 mb
p' = 300 mb

FIGURE 13

III. PROGRAM FOR THE NEXT REPORTING PERIOD

A. Continuing Radiation Budget Research

The preliminary results noted in the previous section will be explored in more detail. Two or three students will complete their individual M.S. theses. We will emphasize interannual variation and separate atmosphere/ocean studies. Potential results are exciting.

B. Opportunities for Use of New Satellite Data Soon to be Available

The objectives of this Grant include cooperation and collaboration in new and future efforts of the Laboratory for Meteorology and Earth Surveys.

In addition to more seasonal radiation budget samples from the MRIR on NIMBUS-III during 1970 and 1971, the multi-channel surface temperature experiment planned for EOS is a prime candidate to acquire more radiation budget measurements from polar orbit. From geosynchronous orbit, the visible and infrared imagers (and perhaps sounders) planned for ATS-F and G and the SMS series will allow valuable study of the complete diurnal cycle of the radiation budget over certain earth areas.

As these experiments will provide definite opportunities for more radiation budget work, we have already tested methods to obtain the total infrared radiant emittance from such data. Using a moderate resolution radiative transfer program ($\Delta\nu = 10\ cm^{-1}$) we have simulated the unfiltered radiance arising over the infrared spectrum (4.3-100 μm) and from within narrower spectral regions chosen to approximate the sensor channels (for example, on EOS). Twenty-one typical atmospheric profiles were used; the U.S. Standard Atmosphere plus the 20 (globally distributed) soundings used in the NIMBUS-III data reduction work. Since nadir angles of view for both 0^o and 30^o were simulated, each satellite experiment was run for 42 different atmospheric conditions. Clouds were not simulated in this preliminary work.

The EOS-SST experiment was run using both broad-band and narrow band channels. In micrometers, the spectral limits were:

Variable	EOS broad-band	EOS narrow-band
X_1	10 - 12	10.75 - 11.25
X_2	8 - 10	8.85 - 10.35
X_3	5.7 - 7.7	6.45 - 6.95
X_4	4.38- 5.9	4.65 - 5.15

For the geosynchronous IR experiments, two channels (those of the THIR on NIMBUS-IV) were chosen as representative:

Variable	ATS-IR
X_1	6.4 - 7.2
X_2	10.3 -12.8

Weighting functions, $d\tau/d \ln p$, and $B \cdot \frac{d\tau}{d \ln p}$ were also computed.

With the sample of N=42 for each of the three cases, a multiple linear (least squares) regression equation was derived with the total infrared radiance as predictand and the experiment channel's unfiltered radiance values as potential predictors. Each predictor was automatically screened by testing its contribution to the reduction of predictand variance. Results thus not only show how well the total IR radiance can be statistically inferred, but also point out the channels most critical for radiation budget work.

For the 42 atmospheric conditions the mean value and standard deviation of the dependent variable (predictand) was 78.72 and 13.80 $w \cdot m^{-2} \cdot Sr^{-1}$ respectively.

Experiment	Standard Error to Total IR radiance ($w \cdot m^{-2} \cdot Sr^{-1}$)	Rank of Channels
EOS-SST (BROAD-band)	0.40	9.1, 6.7, 4.9, 11.0 μm
EOS-SST (narrow-band)	0.73	9.1, 6.7, 11.0 μm
ATS-IR (a la THIR)	1.09	11.5, 6.7 μm

Apparently, the 9.1 μm channel is more useful for radiation budget work with EOS-SST than the 11 μm channel. The O_3 and bit of H_2O, together with the window radiance must be the reason for this.

Further work, with simulated clouds, will be deferred until filter values are finalized for each channel of the respective experiments. Prospects look very good for radiation budget return from the experiments studied. EOS-SST will include a total reflected solar channel for that component of the radiation budget, ATS-Fand G and SMS will have narrower spectrum "visible" channels.

C. Simulation of a New Satellite System for Radiation Budget Measurements

As an eventual follow-on to the radiation budget measurements available from sensors on experimental satellites - a longterm (e.g., 10 year) operational experiment will be required to attack problems of the radiation budget, especially for climate change.

Present accuracies must be improved on three fronts:

a) better radiation budget instrumentation

b) better (less-biased) global sampling in time and space

c) measurement of the solar constant

Point (a) will result from better technology, (c) is planned already, but (b) needs more immediate attention. For a cohesive 10-year experiment several candidate satellite platforms exist. Under Grant auspices (and in collaboration with NCAR) a radiation budget system simulation program has been developed and tested on one candidate platform, the moon. Results of the simulation (see Fig.(14)) encouraged the principal investigator to prepare a proposal for engineering design studies of such an experiment. Submitted to AAFE of NASA, the proposal was not funded although it passed critical science review. A revised version, incorporating improvements and proposing a more general approach regarding platforms for measurements is now in preparation.

Fig. 14

Simulation of Shortwave Solar Radiation Flux Reflected from Earth and Reaching Moon's Surface

Model Time July 2, 1971

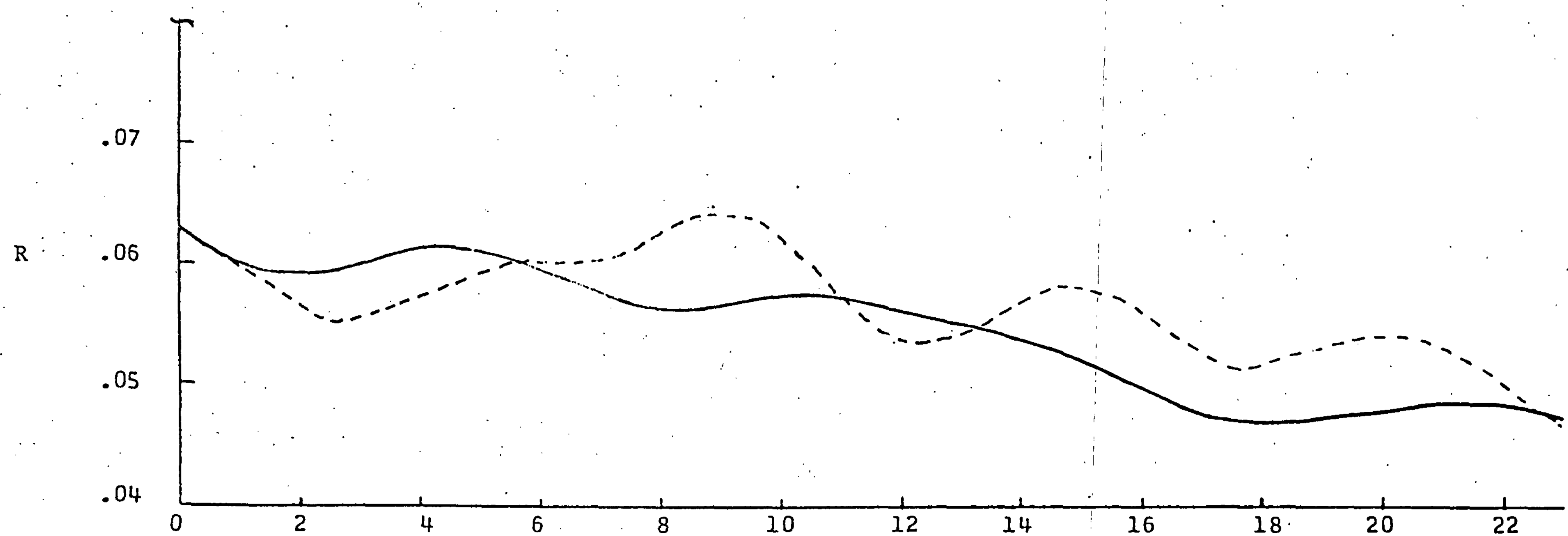

------ 15 day higher-amplitude June 1969 albedo pattern

——— annual (smoothed) albedo pattern

$R \times 2.48 \times 10^{-5}$ watts cm^{-2} = absolute energy flux

Earth's subsolar points	Begin 23.11° Latitude	130.9° E. Longitude		
	End 23.03° Latitude	196.0° E. Longitude		
Earth's sublunar points	Begin -13.4° Latitude	280.3° E. Longitude	}	Moon's positions are approximate
	End -17.8° Latitude	305.3° E. Longitude		

The reflecting surface area of the Earth as viewed from the Moon is decreasing.

IV SPECIAL ACTIVITIES RELATED TO GRANT OBJECTIVES

For the record, this section includes the mention of work by the principal investigator in special areas related to objectives of this Grant and of the Laboratory for Meteorology

- As a corresponding member of Panel B of COSPAR Working Group 6, I have assisted with a study of opportunities to detect global pollutants from a spacecraft; during 1972, in some special meetings, we will continue discussion directed toward studying man's climate and environment problems with the aid of space data systems.

- In working with geosynchronous satellite data, the author has found it essential to develop a radiance normalization technique to allow study of the physical changes in cloud fields on an intra-and inter-daily basis. The method, based on work by Brennon and Bandeen (and Raschke) uses the same bi-directional reflectance matrices used in processing the NIMBUS-III data. See Appendix B for a description of the work.

- NASA automatically maps satellite data onto Mercator and Polar projections. At CSU we have developed a computer mapping method for the Aitoff-Hammer quasi-equal area projection; it will be given to Barksdale of LMES.

REFERENCES

1. Bartman, 1967, University of Michigan report.
2. Brennan and Bandeen, 1970, Appl. Opt.
3. London and Sasamori, 1971, Space Research, Vol. II.
4. Oort, 1971, JAS
5. Raschke, Vonder Haar, Bandeen and Pasternak, 1972, NASA Tech. Note.
6. Sellers, 1965, Physical Climatology.
7. Stamm and Vonder Haar, 1970, University of Wisconsin report.
8. Vonder Haar and Suomi, 1969, Science.
9. Vonder Haar and Suomi, 1971, JAS

Appendix A: 3 December 1971

Papers and Publications During the Reporting Period

1. A preliminary report on heat budget measurements from Nimbus-III was partly supported by this grant. It was presented at the XIIIth Meeting of COSPAR, Leningrad, 1970, and was published this year in Space Research XI (Springer-Verlag) as:

The radiation balance of the earth-atmosphere during June and July 1969 from NIMBUS-III radiation measurements--some preliminary results

by

E. Raschke, T. Vonder Haar, W. Bandeen, and M. Pasternak

2. The very early results of four seasons of Nimbus radiation data were compared to earlier results from other satellites, with METEOR data obtained during the same time period and with calculations in a paper presented at the January 1971 Annual Meeting of the American Meteorological Society:

Global measurements of the energy exchange between earth and space during the 1960's, including latest results from the NIMBUS-III satellite

by

T. Vonder Haar, E. Raschke, M. Pasternak, and W. Bandeen

Publication of these comparisons awaited analysis of a more complete Nimbus data set (see #7).

3. In March 1971 the author presented an invited paper at the Miami Remote Sensing Workshop:

Global radiation budget and cloud cover by satellite measurements

by

T. Vonder Haar

In addition, he served as discussion leader of a section that considered present opportunities and future possibilities for parameterizing the atmospheric energy budget using satellite data. Proceedings of this workshop will be published.

4. An invited paper was presented at the International Solar Energy Society Conference, NASA, GSFC, in May, 1971. This paper presents results of special interest to scientists concerned with the measurement and use of solar radiation. It will be published in Solar Energy.

Measurements of solar energy reflected by the earth and atmosphere, from meteorological satellites

by

T. Vonder Haar, E. Raschke, W. Bandeen and M. Pasternak

5. At the XIVth meeting of COSPAR (Seattle, 1971), in an open meeting of Working Group 6, we formally presented the annual results of the earth's radiation budget measurements from NIMBUS-III. They independently confirmed global results obtained from earlier satellites, while providing the first high area resolution view of energy exchange between earth and space on the annual scale. The paper, to be published in Space Research Vol. 12, is entitled:

The radiation budget of the earth-atmosphere system as measured from the NIMBUS-III satellite (1969-70)

by

T. Vonder Haar, E. Raschke, M. Pasternak and W. Bandeen

6. Drs. Budyko and Flohn kindly invited a paper on the NIMBUS-III results for their Symposium on Physical and Dynamical Climatology, Leningrad, August 1971. The paper, read in the authors absence by Dr. A. Drummond, will be published in the symposium proceedings. It was titled:

Climatological studies of the earth's radiation budget and its variability with measurements of the satellite NIMBUS-III

by

E. Raschke and T. Vonder Haar

7. An invited paper at the Joint Meeting of the German Physical and Meteorological Societies, Essen, October 1971 contained a discussion of the new NIMBUS results within the framework of the earlier satellite measurements, especially with regard to interannual variations. To be published in a German journal the paper was:

Measurements of the energy exchange between earth and space during the 1960's from satellites

by

T. Vonder Haar and E. Raschke

8. In addition to the formal papers and publications, one of the most personally satisfying events of the reporting period was a 90-minute seminar presented in early November 1971 in the invited seminar series of the Geophysical Fluid Dynamics Laboratory, NOAA/Princeton University. Entitled: Measurements of the earth's radiation budget from satellites: Status, prospects and relation to atmospheric energetics, the seminar reiterated both the wide-ranging relevance of radiation budget data to many atmospheric problems as well as the interest of other scientists in these data. This same experience has greeted the author during similar seminars presented in recent years at MIT, NYU, University of Colorado, and Colorado State University.

APPENDIX B.

Radiance Standardization and Normalization Procedures

Since measurements of reflected radiance (brightness) are dependent upon the angular conditions of observation, a standardization and/or normalization technique must be applied to the data before valid relative comparisons can be made.

In practice, a time sequence of measurements of a given surface may be taken under different angular conditions because of:

(a) a relatively long elapsed time interval from beginning to end of the sequence (a sensor mounted on a fixed platform), thus changing ζ and ψ with θ remaining constant; or,

(b) rapid movement of the instrument (on a satellite or aircraft), thus changing θ and/or ψ while ζ remains constant.

Vonder Haar (1969) discusses the proportionality between ATS reflected radiance measurements (also called digital counts or brightness values) and the bi-directional reflectance (ρ). Thus, given a digital count, D, at time, t, and point, p, then:

$$D = K_1 V_o = K_1 K_2 N_r(\zeta,\theta,\psi) = K_1 K_2 \rho(\zeta,\theta,\psi) H_i \cos \zeta \quad , \qquad (1)$$

where K_1 and K_2 are proportionality constants,

V_o = voltage output from the ATS spin-scan camera,

N_r = measured reflected solar radiance,

ρ = effective bi-directional reflectance of the viewed surface, and

H_i = incident solar irradiance (the solar constant).

Let D' be a digital count from the same cloud or surface at (a) $t + \Delta t$ where p = constant, or (b) $p + \Delta p$ where t = constant. Then:

$$\frac{D}{D'} = \frac{K_1 K_2 \rho H_i \cos \zeta}{K_1 K_2 \rho H_i \cos \zeta'} = \frac{\rho \cos \zeta}{\rho' \cos \zeta'} \quad . \tag{2}$$

Equation (2) is the general expression used for comparisons between D and D'. In order to express the ratio ρ/ρ', empirical χ factors were obtained to represent the variation between actual reflectance and Lambert reflectance as discussed in Appendix C.

For the same cloud or surface the directional reflectances (r) are related by:

$$r'(\zeta') = Fr(\zeta) \quad , \tag{3}$$

where $F = \frac{r'(\zeta')}{r(\zeta=0)} \cdot \frac{r(\zeta=0)}{r(\zeta)} = \frac{r'(\zeta')}{r(\zeta)}$.

The F factors include the actual directional reflectance $[r(\zeta)]$ relative to the directional reflectance at solar noon $[r(\zeta=0)]$. The complete list of model values used is shown in Table B-1.

Since $\chi = \frac{r}{\pi\rho}$ and $\chi' = \frac{r'}{\pi\rho'}$, then from equation (3)

$\chi'\pi\rho' = F\chi\pi\rho$ or,

$$\frac{\rho}{\rho'} = \frac{\chi'}{\chi}\frac{1}{F} = \frac{\chi'}{\chi}\frac{r(\zeta)}{r'(\zeta')} \quad . \tag{4}$$

Therefore, from equation (2), $\frac{D}{D'} = \frac{\chi' r(\zeta) \cos \zeta}{\chi r'(\zeta') \cos \zeta'}$ or,

$$D = \eta D' = \left[\frac{\chi'}{\chi} \frac{r(\zeta)}{r'(\zeta')} \frac{\cos \zeta}{\cos \zeta'} \right] D' = \left(\frac{\rho \cos \zeta}{\rho' \cos \zeta'} \right) D' \quad . \tag{5}$$

Through the proper scaling factor, η, it is then possible to compare digital values from identical clouds or surfaces (a) taken at different times, but over the same geographical location, or (b) observed at separate locations but at the same time.

Table B-1

Directional reflectance relative to the value at solar zenith angle of zero degrees for the Nimbus III ocean and cloud models

ζ	Cos ζ	Ocean $\left(\frac{r(\zeta)}{r(\zeta=0)}\right)$	Cloud $\left(\frac{r(\zeta)}{r(\zeta=0)}\right)$
0°	1.00	1.00	1.00
18°	0.95	1.00	1.00
26°	0.90	1.00	1.00
32°	0.85	1.00	1.00
37°	0.80	1.00	1.05
41°	0.75	1.03	1.10
45°	0.70	1.10	1.14
49°	0.65	1.20	1.18
53°	0.60	1.30	1.22
57°	0.55	1.40	1.28
60°	0.50	1.60	1.32
63°	0.45	1.80	1.38
66°	0.40	2.00	1.42
69°	0.35	2.20	1.48
72°	0.30	2.50	1.52
75°	0.25	2.80	1.55
78°	0.20	3.10	1.58
81°	0.15	3.40	1.60
84°	0.10	3.70	1.60
87°	0.05	4.00	1.60

APPENDIX C

Bi-directional Reflectance Models

If the ocean or a cloud were known to reflect solar radiation according to Lambert's Law (i.e., appeared as an isotropic reflector when viewed from different angles over a 2π steradian hemisphere by an instrument of fixed field of view), then the reflecting surface would always have the same "albedo" for a given solar incidence angle and any angle of view.

Since this is known to be not true, then the bi-directional reflectance (ρ, a property of the surface with units of steradians^{-1}) pattern of the surface must be taken into account. Using the following definitions:

$$\rho(\zeta,\theta,\psi) = \frac{\text{reflected radiation in the direction } \theta,\ \psi_2}{\text{incident radiation from a given } \zeta,\ \psi_1} =$$

$$= \text{bi-directional reflectance} \quad , \qquad \text{and}$$

$$r(\zeta) = \frac{\text{reflected radiation in all directions}}{\text{incident radiation from a given } \zeta,\ \psi_1} =$$

$$= \text{directional reflectance} \quad ,$$

where, according to Figure C-1:

ζ = solar zenith angle,

ψ_1 = solar azimuth angle,

θ = satellite zenith angle,

ψ_2 = satellite azimuth angle, and

ψ = $\psi_1 - \psi_2$ = relative solar azimuth angle.

The two reflectances are related through the equation

$$r(\zeta) = \int_0^{2\pi} \rho(\zeta,\theta,\psi)\cos\theta \, d\Omega =$$

$$= \int_0^{2\pi} \int_0^{\pi/2} \rho(\zeta,\theta,\psi)\cos\theta \sin\theta \, d\theta \, d\psi_2 \quad , \qquad (1)$$

where $d\Omega$ represents the solid angle subtended by the sun at the reflecting surface. Since ρ is independent of direction for a Lambertian surface, equation (1) reduces to

$$r = \pi\rho \quad . \tag{2}$$

The isotropic reflectance from a Lambert surface (equation (2)) was then used as a common base from which the actual bi-directional reflectance $[\rho(\zeta,\theta,\psi)]$ was represented. Using observed cloud reflectivities of Brennan and Bandeen (1970) and others, as well as available summaries presented by Raschke et al. (1972), two models of bi-directional reflectance patterns were assembled. The first is an ocean bi-directional reflectance model; the second is a similar model for clouds. Anisotropic factors (χ) were empirically found to represent the bi-directional reflectance of either a water surface or a cloud via the following equation.

$$\chi(\zeta,\theta,\psi) = \frac{r(\zeta)}{\pi\rho(\zeta,\theta,\psi)} \quad . \tag{3}$$

Thus, $\chi < 1$ is indicative of reflected radiance greater than that which would be received from a Lambert surface when viewed under identical angular conditions (ζ,θ,ψ), and vice versa for $\chi > 1$.

The angular dependence of ocean and cloud reflectance was accounted for via the χ factors as shown in Appendix B. In the case of clouds, other reflectance variables related to physical characteristics of the condensed water vapor are also important. Among these are the phase state and size distribution of the condensate, the amount of condensate and cloud thickness (Stamm and Vonder Haar, 1970). In addition, the nature of the underlying surface may affect the observed cloud reflectivities (Bartman, 1967). Direct inclusion of these other variables is nearly impossible; however, the empirical χ observations do represent the integrated result of all relevant factors.

A vertical cross section through the three-dimensional, χ surface of the ocean model used is shown in Figure C-2. A similar cross section through the cloud model is seen in Figure C-3.

Anisotropic factors were formulated for the following ranges of the three critical angles:

1. Solar zenith (ζ),
   a. $0° \le \zeta < 35°$,
   b. $35° \le \zeta < 60°$,
   c. $60° \le \zeta < 80°$;
2. Satellite zenith (θ), $0° \le \theta \le 60°$ for $\Delta\theta$ of $10°$;
3. Relative azimuth (ψ), $0° \le \psi \le 180°$ for $\Delta\psi$ of $30°$ (symmetry was assumed for $180° < \psi < 360°$).

The complete table values of $\chi(\zeta,\theta,\psi)$ which form a layered matrix of 3 x 6 x 6 are given in Tables C-1 and C-2.

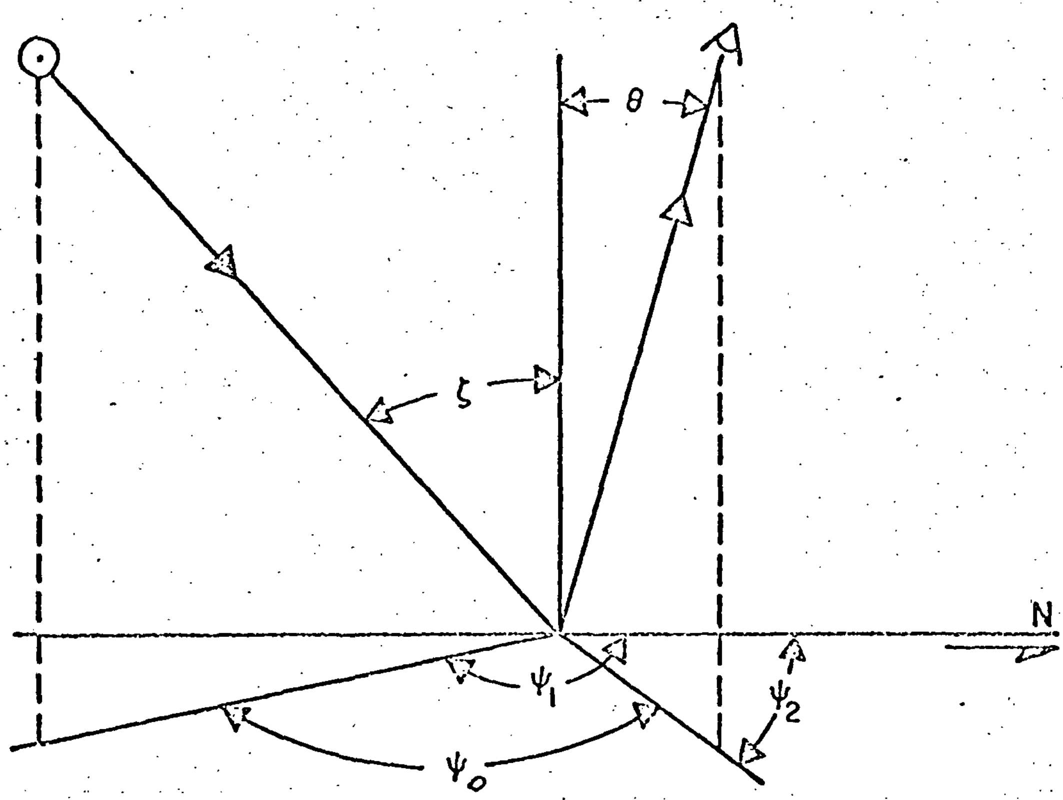

Figure C-1 Geometry of reflectance.

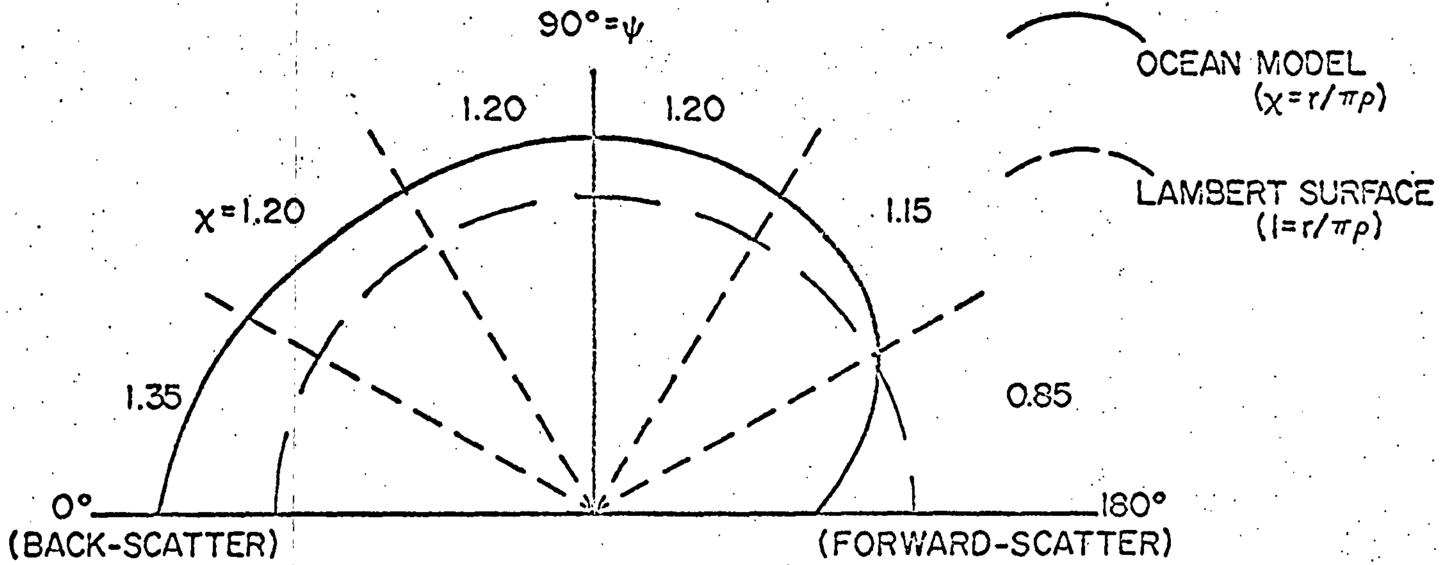

Figure C-2 Vertical cross-section through the χ model for the ocean depicting the difference in reflective characteristics between a Lambert surface and the observed ocean. $\zeta = 35°-60°$, $\theta = 20°-30°$, $\psi = 0°-180°$

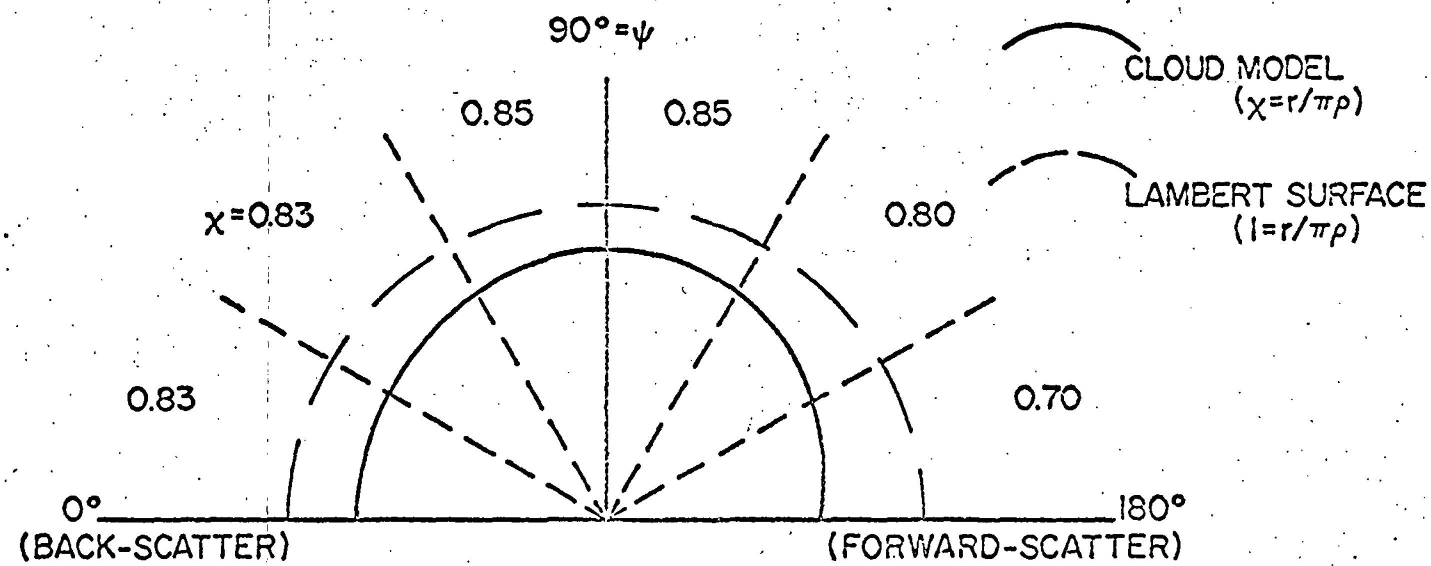

Figure C-3 Vertical cross-section through the χ model for a cloud depicting the difference in reflective characteristics between a Lambert surface and observed clouds. $\zeta = 35°-60°$, $\theta = 40°-50°$, $\psi = 0°-180°$

Table C-1

$\chi(\zeta,\theta,\psi)$ factors for the Nimbus III ocean model

1-A

$0° \leq \zeta < 35°$

θ \ ψ	0°-30°	30°-60°	60°-90°	90°-120°	120°-150°	150°-180°
0°-10°	1.40	1.40	1.40	1.30	1.20	1.20
10°-20°	1.40	1.40	1.40	1.30	1.10	0.80
20°-30°	1.40	1.40	1.40	1.25	0.90	0.50
30°-40°	1.40	1.40	1.40	1.35	0.90	0.50
40°-50°	1.20	1.20	1.25	1.25	1.05	0.70
50°-60°	0.95	1.08	1.12	1.13	1.00	0.60

1-B

$35° \leq \zeta < 60°$

θ \ ψ	0°-30°	30°-60°	60°-90°	90°-120°	120°-150°	150°-180°
0°-10°	1.30	1.25	1.25	1.20	1.20	1.20
10°-20°	1.35	1.25	1.20	1.20	1.20	1.05
20°-30°	1.35	1.20	1.20	1.20	1.15	0.85
30°-40°	1.25	1.10	1.10	1.15	0.98	0.55
40°-50°	1.10	1.05	1.08	1.15	0.95	0.35
50°-60°	1.03	0.90	1.03	1.07	0.80	0.15

1-C

$60° \leq \zeta < 80°$

$$\chi = 0.70 = \text{constant}$$

Table C-2

$\chi(\zeta,\theta,\psi)$ factors for the Nimbus III cloud model

2-A

$0° \le \zeta < 35°$

$\chi = 1.02 = \text{constant}$

2-B

$35° \le \zeta < 60°$

θ \ ψ	0°-30°	30°-60°	60°-90°	90°-120°	120°-150°	150°-180°
0°-10°	1.00	1.00	1.00	1.00	1.00	1.00
10°-20°	0.93	0.93	0.93	0.95	0.95	0.95
20°-30°	0.90	0.90	0.93	0.93	0.93	0.90
30°-40°	0.87	0.87	0.90	0.93	0.88	0.83
40°-50°	0.83	0.83	0.85	0.85	0.80	0.70
50°-60°	0.75	0.75	0.76	0.76	0.68	0.53

2-C

$60° \le \zeta < 80°$

θ \ ψ	0°-30°	30°-60°	60°-90°	90°-120°	120°-150°	150°-180°
0°-10°	1.04	1.04	1.02	1.00	1.00	1.00
10°-20°	1.07	1.04	1.00	1.00	0.98	0.98
20°-30°	1.04	1.04	1.00	0.97	0.93	0.93
30°-40°	0.97	0.97	0.97	0.93	0.86	0.80
40°-50°	0.84	0.87	0.92	0.86	0.74	0.70
50°-60°	0.72	0.78	0.82	0.75	0.64	0.60